Supplementary Information

The Solution Structural Ensembles of RNA Kink-turn Motifs and Their Protein Complexes

Xuesong Shi,[a] Lin Huang,[b] David M. J. Lilley,[b] Pehr B. Harbury[a] and Daniel Herschlag[a,c,d,e]

a, Department of Biochemistry, c, Department of Chemistry, d, Department of Chemical Engineering, e, ChEM-H, Stanford University, Stanford CA, 94305, USA.

b, Nucleic Acid Structure Research Group, School of Life Sciences, University of Dundee, Dundee, DD1 5EH, UK.

Table of Content

Supplementary Results

Supplementary Table 1. Salt conditions used in experiments and controls

Salt condition	NaCl (mM)	KCl (mM)	Na.Asc-orbate (mM)	Tris•HCl, pH 7.4 (mM)	Total mono-valent cation (mM)*	$MgCl_2$ (mM)	Relative salt strength**
1	10	0	10	30	46	0	1.0
2	50	0	10	70	120	0	2.6
2b	150	0	10	70	220	0	4.8
3	0	150	10	70	220	1	5.8
4	500	0	10	70	570	0	12.0
5	50	0	10	70	120	10	12.6
6	150	0	10	70	220	10	14.8

*****At pH 7.4, 1 mM Tris contains 0.86 mM monovalent cation.

** Relative salt strength = [monovalent cation]/46 + [divalent cation], as described in Online Methods and **Supplementary Figure 7**.

Supplementary Table 2. End-labeled probe parameters obtained from optimization of the mean Au-Au distances and Au-Au distance variances of the Au probes by comparison to predictions from a linear elastic rod RNA model.

$MgCl_2$[1]	End labeling probe parameters			
(mM)	D (Å)	$2\theta_0$ (°)	$2axial_0$ (Å)	ε_{Au}
0	6.7 ± 0.3	-57 ± 5	19.2 ± 0.3	0.03 ± 0.04
10	5.5 ± 0.6	-34 ± 15	17.3 ± 0.6	0.01 ± 0.02
	RNA helical parameters (average per base step)[2]			
	Twist (°)	Tilt (°)	Roll (°)	
0	30.8 ± 0.4	-1.9 ± 0.1	5.3 ± 2.9	
10	31.0 ± 0.4	-3.7 ± 2.3	6.8 ± 0.9	
	RNA elastic parameters[2]			
	B (bending persistence length, nm)		C (twisting persistence length, nm)	
0	62 ± 9		45 ± 19	
10	83 ± 29		29 ± 16	

End-labeled probe parameters in this table were obtained by comparing the observed mean Au-Au distances and Au-Au distance variances with predictions from a linear elastic rod model of RNA (X.S., P.B.H. and D.H., paper in preparation) analogous to that for DNA[2]. The best-fit parameters were determined by numeral search using MATLAB and the errors reported are 66% confidence interval.

[1] Common experimental conditions are: 50 mM NaCl, 10 mM Na•Ascorbate, 70 mM Tris•HCl, pH 7.4.

[2] Estimated using Equation (1), the values in **Supplementary Table 1** above, and the parameters from (X.S., P.B.H. and D.H, paper in preparation).

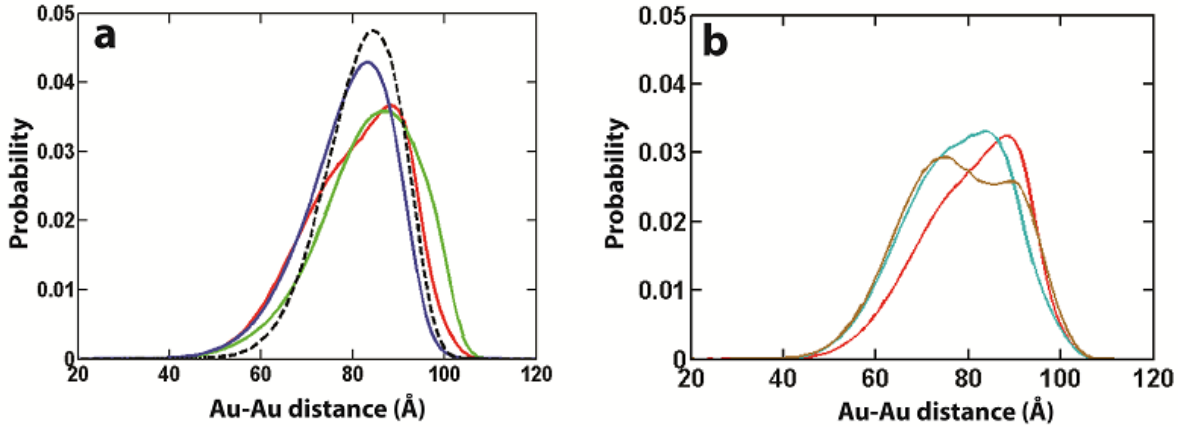

Supplementary Figure 1. Comparison of the predicted Au-Au distance distribution for Tar RNA (blue) and the unkinked state of KtA (green) and KtB (red). The Tar RNA distribution (blue) is predicted using Tar ensemble from (ref. 1). Also plotted is the predicted Au-Au distance distribution for a single bulge conformation (black dashed line). The Au-Au distance distributions for the unkinked states of KtA under salt condition 2 (**a**, green) (**Supplementary Table 1)** and KtB under salt conditions 2 (**a** and **b,** red), 3 (**b**, cyan) and 5 (**b**, brown) (**Supplementary Table 1)** were obtained by first decomposing the experimental distribution into contributions from kinked and unkinked basis set structures (e.g. **Fig. 2b**), and then renormalizing the unkinked contributions to a total probability of 1. The mean Au-Au distances plotted do not account for the small variation in Au probe position in the different salt conditions and instead uses the expected position for salt condition 2 (**Supplementary Table 1**) in order to remove this additional variable and allow direct comparison of these ensembles under different salt conditions.

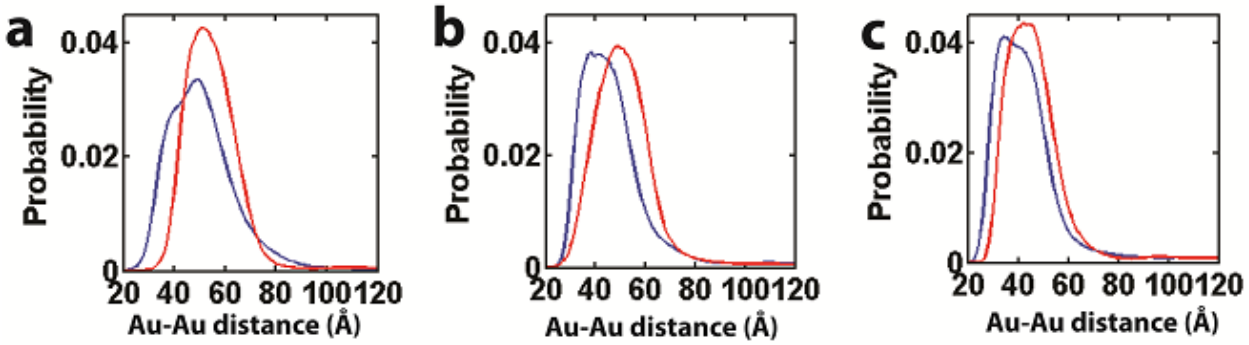

Supplementary Figure 2. The KtA• L7Ae and KtB• L7Ae kink-turn conformational states differ. The measured Au-Au center-to-center distance distribution for KtA (blue) and KtB (red) with excess L7Ae under solution conditions of **(a)** 70 mM TrisHCl, pH 7.4, 10 mM sodium ascorbate and either 50 mM NaCl (low salt; condition 2 in **Fig. 2** and **Supplementary Table 1**), **(b)** 150 mM KCl and 1 mM $MgCl_2$ (intermediate salt; condition 3 in **Fig. 2** and **Supplementary Table 1**), or **(c)** 50 mM NaCl and 10 mM $MgCl_2$ (high salt; condition 5 in **Fig. 2** and **Supplementary Table 1**).

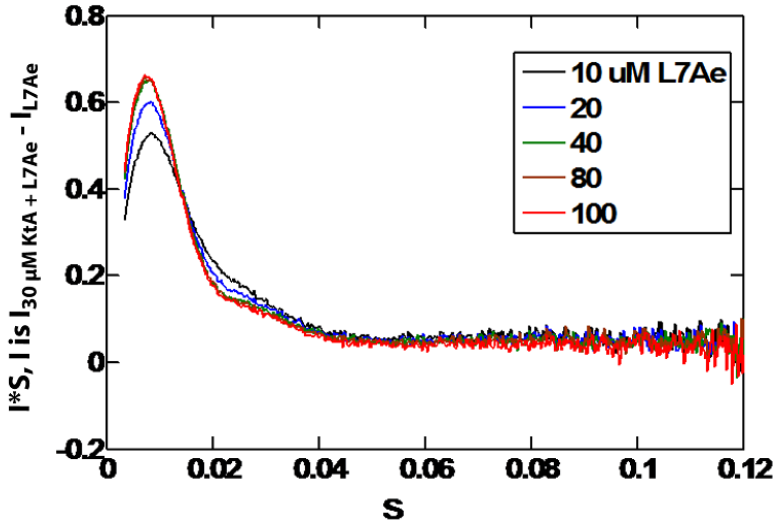

Supplementary Figure 3. **SAXS titration of 30 μM of KtA with 10 to 100 μM L7Ae**. Solution conditions: 50 mM NaCl, 10 mM NaAscorbate and 70 mM TrisHCl, pH 7.4 (condition 2 in **Supplementary Table 1**).

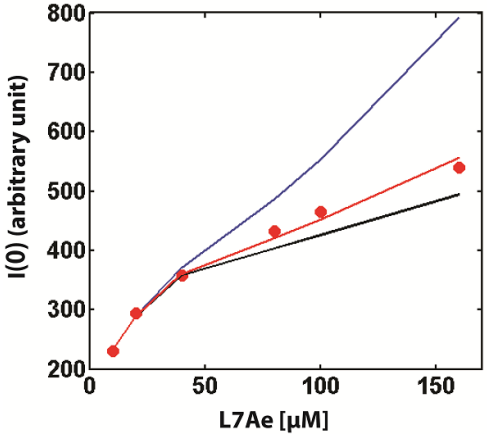

Supplementary Figure 4. The amount of non-specifically bound L7Ae under XSI condition is insignificant. The relative change in the experimental I_0 values at different L7Ae concentrations (red filled circle, solution condition: 50 mM NaCl, 10 mM NaAscorbate, 70 mM TrisHCl, pH 7.4, and a constant KtA concentration of 30 μM) are plotted together with predicted I(0) values assuming there is non-specific binding of L7Ae to RNA with $K_{d,\text{non-specific}}$ of 0.39 mM (blue line), 2 mM (red line) or there is no non-specific binding of L7Ae to RNA (black line). The data are consistent with the model corresponding to the red line, which predicts that under XSI experimental condition of 30 μM RNA and 100 μM L7Ae, an insignificant fraction (about 3%) of the RNA has non-specifically bound L7Ae. This amount is not expected to alter the conclusions herein. The relative I_0 of RNA with 0 to 2 bound L7Ae were estimated using the FoXS webserver[2].

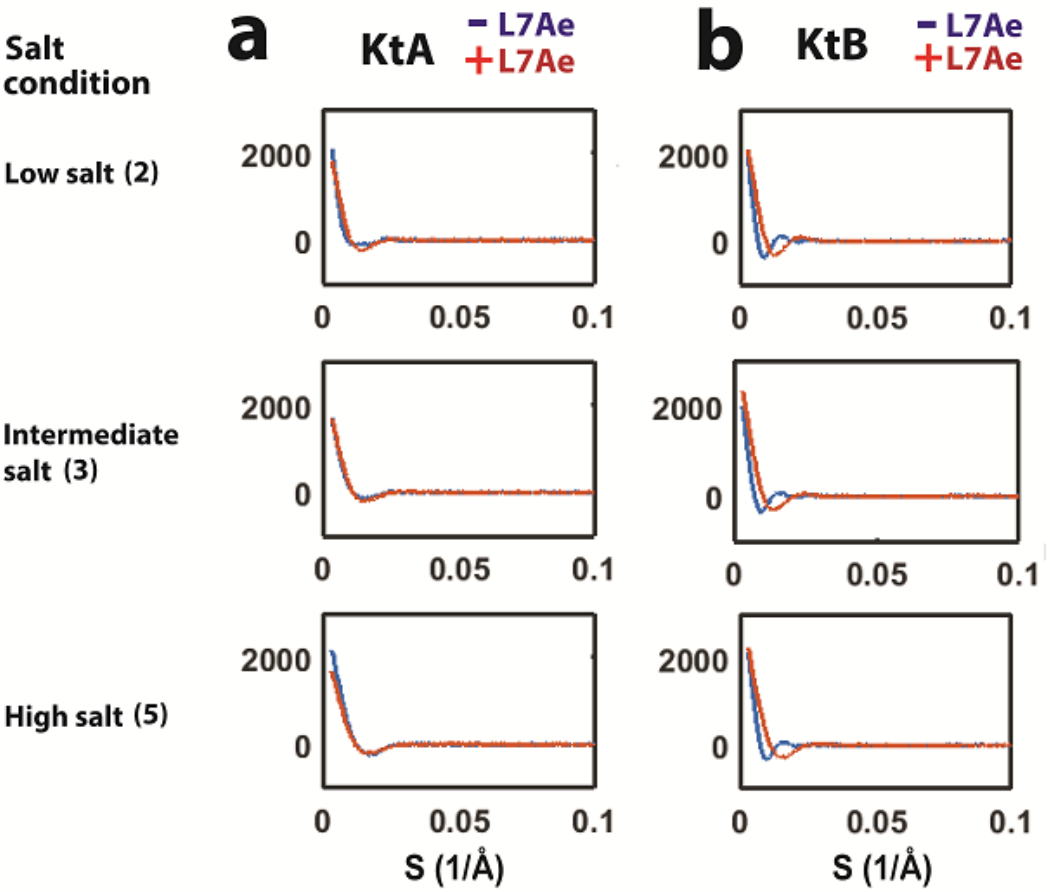

Supplementary Figure 5. The KtA and KtB kink-turn Au-Au scattering profiles without and with L7Ae. The measured Au-Au scattering profiles for KtA (**a**) and KtB (**b**) without (blue) and with (red) bound L7Ae in 70 mM TrisHCl, pH 7.4, 10 mM sodium ascorbate and either 50 mM NaCl (low salt; condition 2 in **Fig. 2** and **Supplementary Table 1**), 150 mM KCl and 1 mM $MgCl_2$ (intermediate salt; condition 3 in **Fig. 2** and **Supplementary Table 1**), or 50 mM NaCl and 10 mM $MgCl_2$ (high salt; condition 5 in **Fig. 2** and **Supplementary Table 1**). See **Figure 4** for the corresponding Au-Au center-to-center distributions.

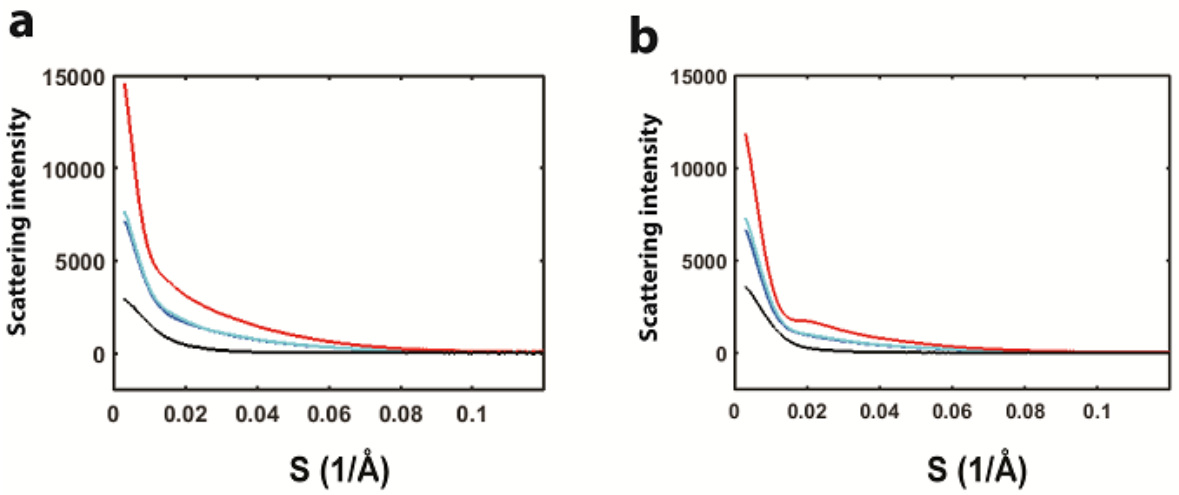

Supplementary Figure 6. Representative SAXS data sets used for obtaining XSI profiles. Each SAXS dataset of KtB (**a**) and KtB.L7Ae (**b**) under salt condition 2 (**Supplementary Table 1**) contains SAXS profiles for constructs without (black) and with single (blue and cyan) or double (red) gold nanocrystal labels. The profiles for KtB.L7Ae are after the subtraction of minor scattering contributions from free L7Ae, calculated using separately measured SAXS profiles of L7Ae alone. Each set of four profiles was used to calculate the Au-Au scattering profile or the XSI profile (**Supplementary Fig. 5b** low salt) using previously established procedures[3, 4].

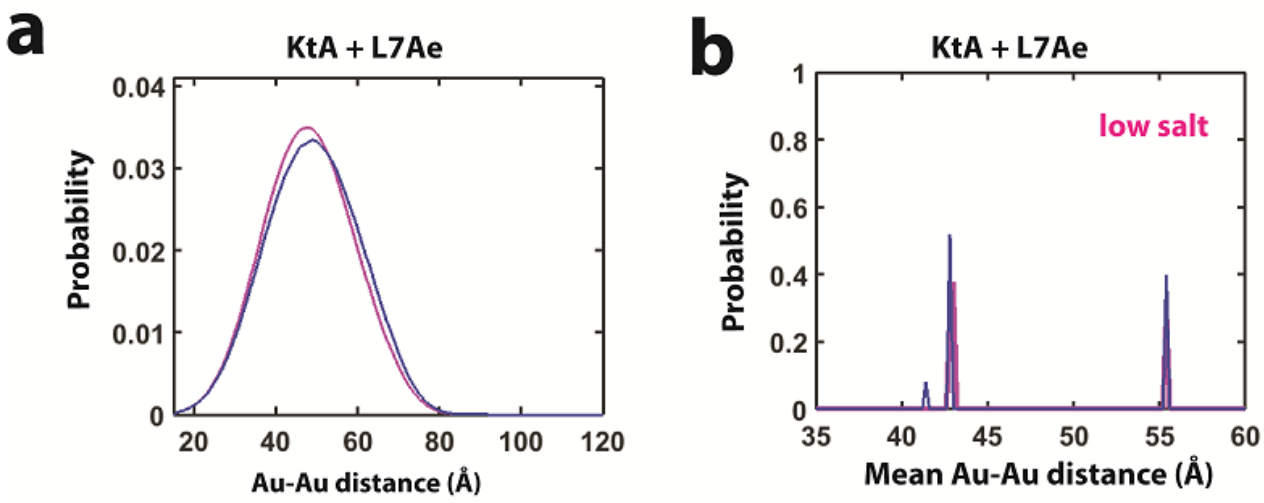

Supplementary Figure 7. Independent repeated measurements of the kinked KtA•L7Ae. (**a**) The normalized Au-Au center-to-center distance distribution of the kinked KtA•L7Ae and (**b**) the probability distribution of the kinked ensemble for KtA•L7Ae under salt condition 2 (**Supplementary Table 1**). Magenta (**a**, **b**) are replotted from **Figure 5a** (magenta, normalized solid line) and **Figure 5e** (magenta), respectively. Blue (**a**, **b**) are from a repeated measurement using independently prepared RNA samples.

Supplementary Figure 8. RNA sequences used in determining the Au nanocrystal parameters for 3′ end-labeled Au nanocrystals. Au nanocrystals (orange sphere) were either internally attached at guanines through a N2-amino-C6-dG modification (Glen Research) or 3′ end-labeled using a C3 3′-thiol modification (Glen Research).

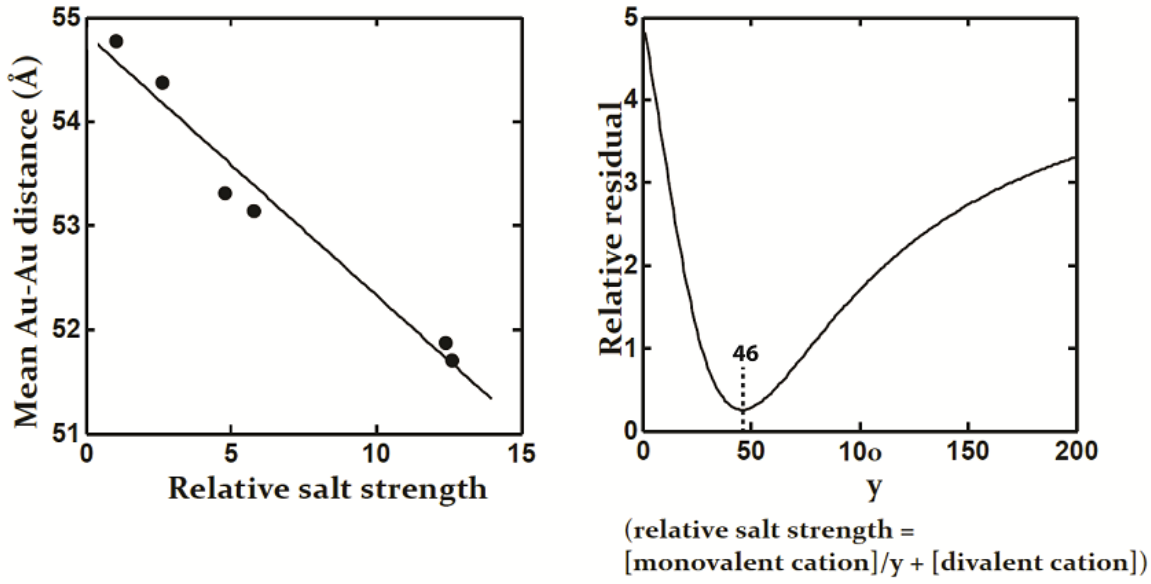

Supplementary Figure 9. Use of the salt dependence of the mean Au-Au distance of an end-labeled RNA helix to define a relative salt strength scale. The salt dependence of the mean Au-Au distance of a 12bp RNA helix with end-labeled Au nanocrystals (condition 1 to 6 in **Supplementary Table 1**; see **Supplementary Fig. 8**, construct 2 for sequence) is linear when the relative salt strength of the solution (left panel) and defined as [monovalent cation (mM)]/46 + [divalent cation (mM)]. The value 46 was determined to give the best linear fit. The right panel depicts the residuals for fits to the left panel and gives 46 as the best-fit value.

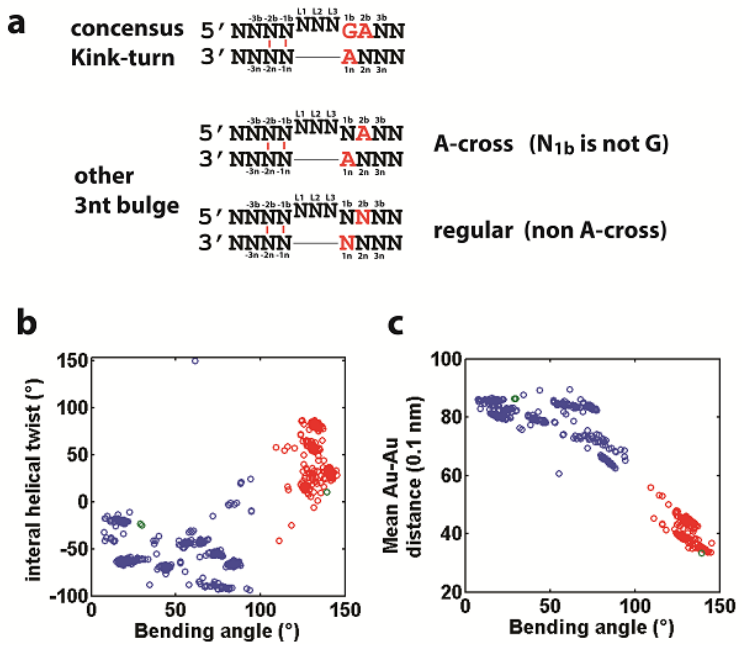

Supplementary Figure 10. Survey of kink-turn and other 0-3 two-way junctions in the crystal structure database. (a) 0-3 two-way junctions with a canonical or near canonical 5′-stem are distinguished by their 3′-stem sequences as being a kink-turn, an A-cross, or a regular 3nt-bulge. See Online Methods for details. **(b)** The distribution of inter-helical orientations for the consensus kink-turn sequences (Red), A-cross bugle (green) and other 3nt bulge sequences (blue). **(c)** The bending angles are correlated with the expected mean Au-Au distances in the context of the experimental construct herein (**Fig. 1b**). Color-coded as panel **b**.

.

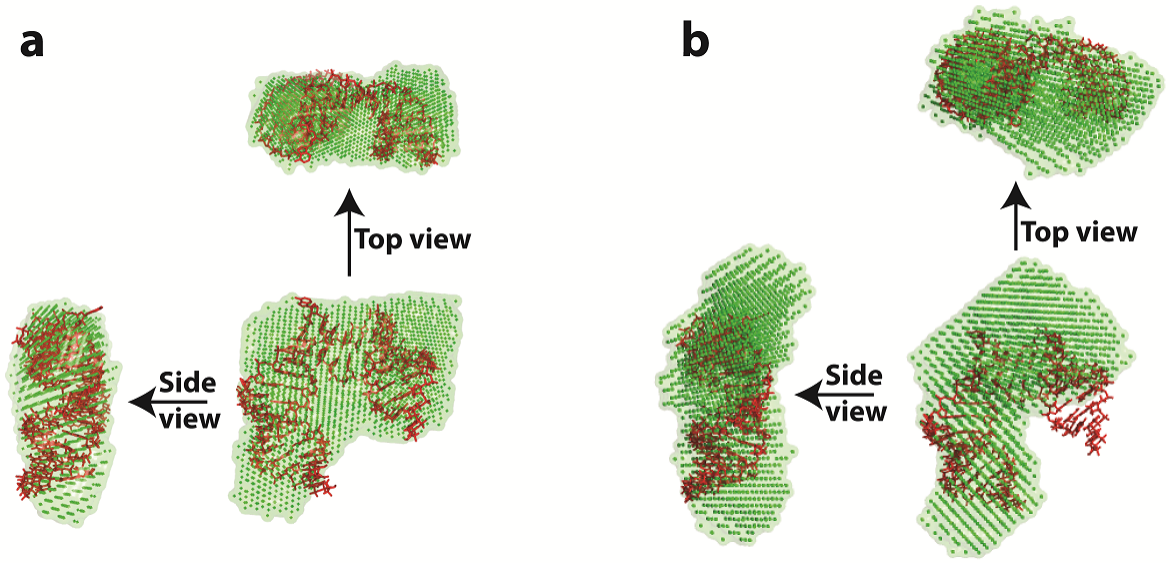

Supplementary Figure 11. Comparison of the SAXS envelope of KtA with its crystal structure model. The SAXS envelopes of KtA RNA (green) under the (**a**) high salt (condition 5 in **Supplementary Table 1**) and (**b**) low salt (condition 1 in **Supplementary Table 1**) conditions were constructed using DAMMIN[5]. A structural model of the full size experimental KtA construct (red) based on crystal structure 4BW0 was manually positioned to fit the envelope, giving a reasonable fit at high salt (**a**) but not low salt (**b**), as expected.

References

1. Salmon, L., Bascom, G., Andricioaei, I. & Al-Hashimi, H.M. A general method for constructing atomic-resolution RNA ensembles using NMR residual dipolar couplings: the basis for interhelical motions revealed. *J. Am. Chem. Soc.* **135**, 5457-5466 (2013).
2. Schneidman-Duhovny, D., Hammel, M., Tainer, J.A. & Sali, A. Accurate SAXS Profile Computation and its Assessment by Contrast Variation Experiments. *Biophys. J.* **105**, 962-974 (2013).
3. Mathew-Fenn, R.S., Das, R. & Harbury, P.A. Remeasuring the double helix. *Science* **322**, 446-449 (2008).
4. Shi, X., Herschlag, D. & Harbury, P.A. Structural ensemble and microscopic elasticity of freely diffusing DNA by direct measurement of fluctuations. *Proc. Natl. Acad. Sci. USA* **110**, E1444-1451 (2013).
5. Svergun, D.I. Restoring low resolution structure of biological macromolecules from solution scattering using simulated annealing. *Biophys. J.* **76**, 2879-2886 (1999).